Applied Surface Science 579 (2022) 152138

Contents lists available at ScienceDirect

Applied Surface Science

journal homepage: www.elsevier.com/locate/apsusc

Full Length Article

Insights on the effect of water content in carburizing gas mixtures on the metal dusting corrosion of iron

El Tayeb Bentria [a], Salawu Omotayo Akande [b], Abitha Ramesh [c], Nicholas Laycock [c], Wouter Hamer [d], Mousseau Normand [e], Charlotte Becquart [f], Othmane Bouhali [b], Fedwa El-Mellouhi [a,*]

[a] Qatar Environment and Energy Research Institute, Hamad Bin Khalifa University, Doha P.O. BOX 34110,Qatar
[b] Texas A&M University at Qatar, Doha P.O. Box 23874, Qatar
[c] Qatar Shell Research and Technology Center, QSTP, Doha, Qatar
[d] Shell Technology Centre Amsterdam, Netherlands
[e] Département de physique and Regroupement québécois sur les matériaux de pointe, Université de Montréal, Montréal QC H3C 3J7 Canada
[f] Univ. Lille, CNRS, INRAE, Centrale Lille, UMR 8207 - UMET - Unité Matériaux et Transformations, Lille F-59000, France

ARTICLE INFO

Keywords:
Metal dusting corrosion
Molecular dynamics
Reactive Force Field
Surface reaction
Syngas

ABSTRACT

Constituents of syngas, such as water, carbon monoxide and sulfides, can cause the degradation of the steel pipes they move through, leading to carbon dusting and corrosion. In spite of considerable attention to this process, many questions remain about its origin. We conduct reactive molecular dynamics simulations of multi-grain iron systems exposed to carburizing gas mixtures to investigate the effect of water content on metal dusting corrosion. To simulate carbon monoxide (CO) dissociation followed by carbon diffusion, we employ an extended-ReaxFF potential that allows accounting for both the high C atoms coordination in bulk iron as well as the lower C coordination at the iron surface and interfaces. The reactions happening in the sample at different water concentrations and at different time frames are explored. We demonstrate that the presence of water on a clean Fe surface promotes different catalytic reactions at the beginning of the simulations that boost the C, H, O diffusion into the sample. At later stage, the formation of oxide scale leads to an elevated concentration of H_2O/OH molecules on the surface due to the decrease in Fe affinity to dissociate water. This results into blocking the Fe catalytic sites leading to lower C and O diffusion to the bulk of the sample.

1. Introduction

Water and varying amounts of carbon monoxide and sulfides are among the constituents of syngas that affect the integrity of mild steel pipes as it flows through them [1]. More specifically, this phenomenon is associated with carbon deposition that leads to the internal corrosion of pipelines and syngas production in systems made from mild steel. The corrosion observed here is associated with the decomposition of structural materials into dust of metal particles in strongly carburizing atmospheres and represents an economic challenge for the oil and gas industry [2]. Beyond this simple description, the so-called metal dusting corrosion takes many forms depending on gas concentration, alloy composition, surface treatment, and carbon activity on the material involved. For instance, in reformer environments under operating conditions, the incubation time of metal dusting attack is determined by a competition between the oxide scale development that depends on water concentration and deposition, and penetration of carbon from decomposed CO molecules [3]. Furthermore, a report by K. Natesan et al. [3] showed that the local nature of dusting initiation on both Fe- and Ni-based alloys are governed also by the presence of defects within the oxide scales such as pits. They also reported that oxide scaling may not occur if carbon activity is higher than 1 ($a_c > 1$) and if the H_2O content in the environment is very low. Along the same line, water was reported to promote a carburization attack on a clean iron surface by providing favorable conditions for various surface reactions. This effect was found to decrease upon increased metal oxidation [4,5].

Grabke *et al.* [2] studied the carburization of low alloy steel (1 %Cr-0.5 %Mo) exposed to a flowing CO-H_2-H_2O gas mixture at atmospheric pressure and $a_c > 1$, operated at temperature T = 773 K. The rate of metal loss was determined by analyzing the corrosion products after

* Corresponding author.
E-mail address: felmellouhi@hbku.edu.qa (F. El-Mellouhi).

https://doi.org/10.1016/j.apsusc.2021.152138
Received 2 September 2021; Received in revised form 4 November 2021; Accepted 3 December 2021
Available online 7 December 2021

exposure to these molecules. They concluded that metal dusting was inhibited but could not be suppressed by increasing the oxygen activity or peroxidation; they remarked that after rapid oxidation, a very slow but steady oxide growth follows. Overall, they found that while increasing the CO and H_2 partial pressure promotes metal dusting, water is associated with a significant inhibition of dusting corrosion.

Despite these findings and many other experiments, there is still a large gap between the experimental observations and the fundamental understanding of the catalytic processes governing these carbon dusting. Here, numerical simulation can help. Density Functional Theory (DFT) calculations can capture the key chemical reactions of molecules on surfaces [6] and have been used to study reaction of water on clean iron surfaces [7,8]. Rafael *et al.* calculated the energetics of water and hydroxyl groups (OH) adsorption and dissociation of on Fe(1 0 0) surface [4]. They showed that water is weakly adsorbed on top sites and dissociates by overcoming a barrier of 1 eV, while after losing a hydrogen, the remaining OH gets attached to the surface with a 0.8 eV dissociation barrier for the second hydrogen atom. Ashriti *et al.* described the formation of water on Fe(1 0 0) surface by hydrogenation, with a barrier, they found, of + 1.99 eV, making it thermodynamically unfavorable. Shaoli *et al.* studied the coverage dependent of H_2O, OH, O, and H adsorption and dissociation and showed that the H_2O dissociation barrier can go as low as 0.32 eV for the Fe(1 1 1) surface with $4O + H_2O_{(s)} + 4H_{2(g)} + 4H_2O(g)$ system for example, proving that the practically complex chemical reactions could drastically change the barriers on Fe surface [9]. Despite these insights from DFT simulations, especially regarding the very early stages reactions leading to metal dusting corrosion, their high computational costs have limited their application to the more relevant time and length scales. These limitations make it difficult to observe the effect of competing dissociation mechanisms due to mutually adsorbed syngas molecules on iron surface at high temperature. Larger-scale simulations, such as mesoscale, continuum, and the micro-kinetics, offer valuable tools to probe the overall reactions and analyze their corresponding products. However, results from these studies strongly depend on the inserted parameters taken from either existing simulations or experiments and can lead to biased or incorrect conclusions. Moreover, these approaches have limitation in capturing the fundamentals of corrosion initiation due to their dependence on atomic level reactions inserted [10].

Atomistic simulation methods such as molecular dynamics are powerful tools for exploring, developing, and optimizing the properties of materials. Force field molecular dynamics simulations offer a good compromise over DFT by enabling the use of systems containing thousands of atoms that can be followed over nanoseconds and more. Atomistic mechanisms developing over larger scales are indeed essential to explain the effect of water content in syngas on C diffusion in iron systems, a phenomenon that is still largely unexplored. Among those, the reactive force fields (ReaxFF potentials), a computationally reasonable bond-order-dependent potential that includes Van Der Waals and Coulomb forces, is of particular interest. Several parametrized versions of ReaxFF potentials suited for specific applications that enable to tackle the complex surface chemistry of hydrocarbons on iron surfaces have been proposed [11,12,13]. Recently we showed that ReaxFF, with its conventional formalism, struggles to predict correctly the iron carburization that requires that C moves from a low-coordinated surface environment to a higher coordinated bulk state. We lifted this limitation, extending the standard parameter setup to allow specific adaptation to the interactions of carbon at the surface and in the bulk separately, and constructing an Extended-ReaxFF [14]. In this work, we investigate using, molecular dynamics (MD) and our Extended-ReaxFF [14] the impact of water content in syngas on the carburization process of iron slabs: an initial step for initiating metal dusting corrosion. This allows us to consider phenomena dependent not only on the reactivity of the involved species, but also on dynamic factors, such as dissociation, diffusivity and solubility, allowing to probe how atomic species such as H, O, C migrate through the metallic sample [10]. Our recently developed potential enables us to account for the effect of water on metal dusting corrosion. An effect that has not and could not be treated correctly by ReaxFF due to the limitations of the earlier versions [14].

2. Computational details

A periodic simulation box consisting of an iron slab measuring 40x40x40 Å and containing 5115 Fe atoms is used under isothermal–isobaric ensemble (NPT). The surface of the slab is perpendicular to the z-direction to enable the solid–gas interaction via a 50 Å vacuum region filled with a flowing syngas. We perform a benchmarking of the size versus CPU time, pressure and temperature equilibration to identify the appropriate size of the simulation box (see figure S1 in the supplementary). We find that the 5115 Fe atom system was sufficient to offer the best compromise between reasonable computational cost and enough to capture system vibration at high temperature. Figure S1 shows the temperature of pressure stability test for all samples during the simulation, we can see that the temperature fluctuation is ± 25 K, and pressure fluctuation is around ± 2 GPa which corresponds to a ± 1% fluctuation in lattice parameter. Both values are in the accepted range for this type of solid/gas MD simulation at 773 K.

Molecular dynamics simulations are performed using the Large-scale Atomic/Molecular Massively Parallel Simulator (LAMMPS) code [15]. We use the "deposit" command within the LAMMPS package to insert molecules into the vacuum region with an initial speed parallel to the surface. This feature simulates a syngas flow by allowing us to insert molecules randomly in space every N time steps at position at least 10 Å away from the surface and its periodic counterpart in order to avoid collisions due to inserting particles too close to the surface. Fig. 1 shows the atomic model after a simulated time of (a) 50 ps and (b) 400 ps. A carbon atom is considered to have diffused in the bulk if it is at least 2 Å below the surface, i.e., has a z-axis coordinate lower than 38 Å. Controlling the insertion rate is very important as it enables us to monitor and control the concentration of the gas mixture. The biggest challenge we face by using this method is the difference in the reactivity of gaseous species toward the metallic surfaces through time. This might lead to a build-up of excess molecules of certain types in the vacuum leading to an increase in the syngas pressure. Grand Canonical Monte Carlo (GCMC) would be perfect to add/delete molecules and keep a constant gas content and pressure, however it is not supported using ReaxFF formalism. Thus, after trial and error tests of evolution of molecules concentration in this system, we insert molecules at varying rate to keep approximately constant the required concentration (see figure S6). For example, H_2 reactivity is much lower than CO and H_2O in both systems, and it is not recommended to change the setting during the calculation, thus we stop insertion earlier than CO and H_2O molecules to keep H_2 concentration in the gas approximatively around 54% in all systems. To keep the 15% concentration for H_2O, 20% CO and 54% H_2, we use the following insertion rates: insert 300 CO molecules with 2500 fs/particle, only 270 H_2 molecules with insertion every 1500 fs/particle and 225 H_2O from 3333 fs/particle. Finally, we also insert argon atoms to control the gas pressure in the system. The initial gas mixture obtained in our simulations is close to the experimental syngas in plants such as pearl gas-to-liquid (GTL) which is composed of a mixture of gases: H_2 (54%), CO (15%), CO_2 (5%), CH4 (10%), steam (10%), and trace amounts of other compounds (Reformer outlet gases) [3].

We give an initial speed of 0.001 Å/fs to all molecules, corresponding to 100 m/s, parallel to the surface. This is the maximum speed flux used generally in controlled pipelines [16]. After an NPT relaxation of the system at 1 K, we heat up the system by 0.01 K per step to the required temperature (773 K) under microcanonical ensemble (NVE). We relax it for 10,000 steps then start inserting molecules under NPT conditions, which show high stability for large-scale systems.

It was shown by Broos *et al.* [17] that different surface orientations lead to different mechanism for CO dissociation for Fe_3C. While (1 0 1) (1 1 1) favor direct dissociation, other orientations lead to H-assisted CO

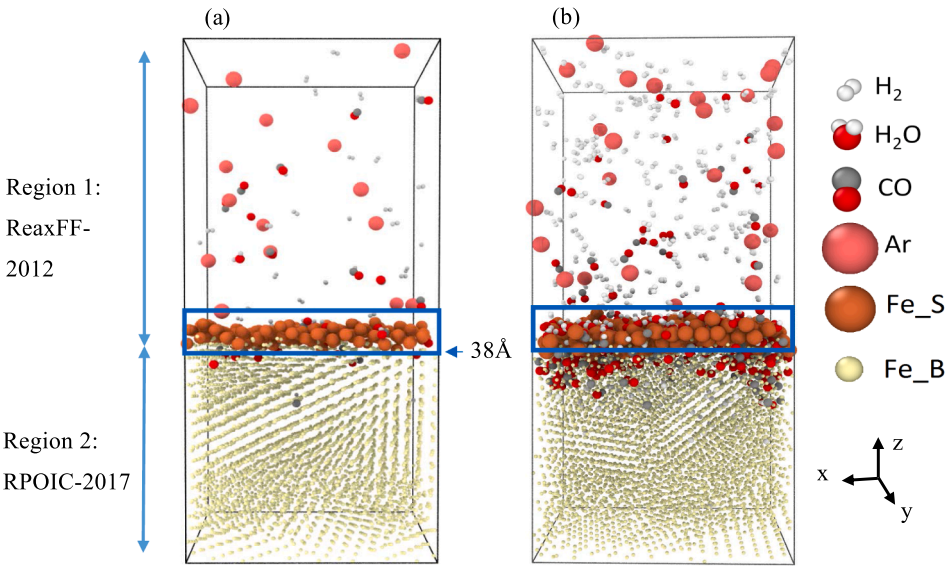

Fig. 1. Computational ball model used in this work after a simulated time of (a) 50 ps and (b) 400 ps in the presence of a H_2O, CO_2, H_2, Ar gas mixture. In the extended ReaxFF formalism used here, iron atoms in the slab are classified as follows: surface iron layer is labelled as Fe_S (in brown). The remaining iron atoms in the bulk are labelled as Fe_B (in yellow). Color codes are as follow: carbon is grey, oxygen is small red, hydrogen in white and Ar in pink. The rectangular blue area represented surface region. Figure generated using OVITO [21].

hydrogenation pathways such as (100), (010), and (01–1) surfaces. Hence, we use a six-Fe-grains model cleaved along (001) axis. This configuration present different surface orientation in the same sample, as well as a diversity of step edges and emerging grain boundaries to the surface (fig. 1). Previous published work [18] demonstrate that multi-grain boundary systems promote the CO dissociation which is the rate limiting step for the carburization process offering a closer scenario to real conditions compared to a perfect surface. Figure S2 shows a snapshot of the Fe surface used in this work. Experiments demonstrate that the dusting corrosion process has a strong dependence upon temperature, which affects the reaction pathways. We use 773 K (500C), the same temperature applied in Grabke *et al.* experiments [19], which represents the critical temperature before entering to the high metal dusting corrosive regime range (773–1073 K) avoided experimentally [20].

3. Results and discussion

We examine the effect of varying water concentration at the early stages of iron corrosion by analyzing the MD results. We use industrial condition of temperature and syngas concentration [22] in building our simulation model. In this section, we analyze different time frames of the simulation as the system evolve to explain the reactions happening, strengthening our results with existing DFT and ReaxFF work on this subject. Finally, we consolidate the general observation on the system with diffusion rate calculation, linear distribution function (LDF) and relative charge map.

Fig. 2 illustrates the number of carbon atoms that diffuse from the surface to the bulk as a function of simulation time, for 0 %, 3 %, 9 % and 15 % water concentration in a gas mixture of 20 % CO, 54 % H_2 filled with Argon. We choose three simulation time frames to describe our simulation, F1: 0–200 ps, F2: 200–400 ps and F3: 400–800 ps. The simulation time reaches 800 ps and is averaged over three runs; the shadowed area colored with respect to each concentration represents the MD fluctuation resulting from the three MD runs with the diffusion average associated with each concentration as a solid line. The MD fluctuations were calculated as the standard deviation of the three runs divided by the square root of the sample size. These give a measure of the sample-to-sample variability of the sample means. One may note from Fig. 2 that the number of carbons having reached the bulk decreases in the presence of water as compared to the case without, in agreement with the experimental observation mentioned earlier. However, we observe weak effect of concentration on carbon diffusion: the

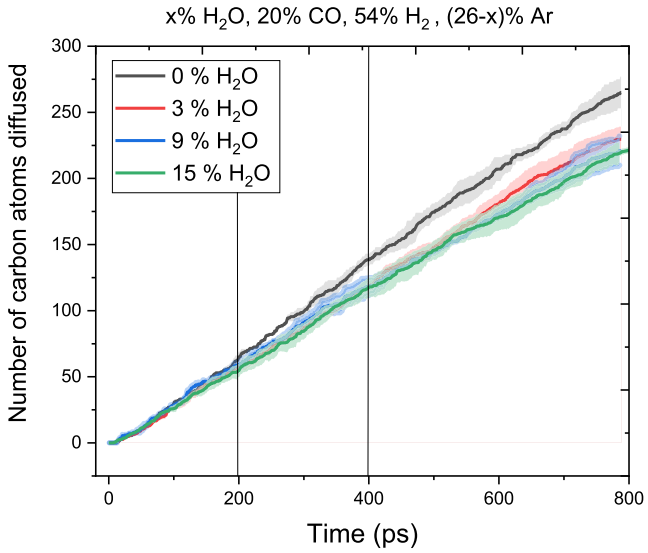

Fig. 2. Number of carbon atoms having diffused into the bulk as a function of time (in ps) for systems containing different water concentrations, 0%, 3%, 9% and 15%, at T = 773 K. For each initial water concentration, the carbon counts within the bulk are averaged over three MD runs (colored solid lines), the shaded area with the same color represent the spread in results over these three MD simulations.

MD fluctuations associated with each run are larger than the difference of the C having diffused for water concentration of 3%, 9% and 15%. In order to understand more the effect of water concentration, Figure S3 shows a pie chart of the fraction of atoms in the bulk, surface and vacuum, at 800 ps and at different water concentrations, that was generated from a single run for each system. We can see clearly that the presence of any amount of water leads to more carbon atoms on the surface compared to the case without water namely 17 % to 24.7–25.7% respectively. This suggests that an increased tendency for C to bind at the Fe surface, as single atom or molecule, reducing the diffusion into the bulk in the presence of water, together with formation of rich oxygen gas as observed in the vacuum region (supplementary S3). The presence of 3% of water leads to an increase of oxygen content in the vacuum from 3.0% to 11.1% compared to the case without water at 800 ps. This suggests, even at small concentration, water can trigger catalytic

reactions on the Fe surface. Since all water concentrations give similar results, in the following, we discuss and analyze two cases only: without water (0 %) and with 15 % water. The main results are also presented for the two other water concentrations in supplementary material.

Fig. 3 represents the fraction of atoms and molecules at the surface for these two systems. This fraction is obtained by dividing the number of target molecules on the surface by the total number of atomic constituent species in the system. We can see from Fig. 3 that the fraction of molecules on the surface to the total number of inserted molecules decreases with time, which is expected as we insert more molecules to react with the same surface through time. The amount of CO and H_2 molecules adsorbed on the surface (*) are denoted as CO* and H_2* respectively. The fraction of CO* and H_2* for the 0% water case is always higher than in the 15% water system. Conversely, the fraction of OH* and hydrocarbons for the 0% water case is always lower than in the 15% water system. The fraction of CH* in the 0% water is higher than 15% water in (200 ps-400 ps, Fig. 3(a-b)), before it inverses at 800 ps (Fig. 3-c). Finally, the formation of H_2O, CO_2 molecules on the surface was not observed in the case without water. Fig. 4 represents the fraction of atoms in Fe bulk at the end of each time slice (200, 400 and 800 ps). This number is calculated by dividing the number of the diffused atoms by the number of inserted atoms for each type. In Fig. 4 we present the fraction of atoms at the bulk for these two systems. We see that it does not decrease through time as the bulk is able of adsorbing the newly inserted molecules. We see also that the amount of C, H, O atoms having diffused into the bulk is larger in the water system comparing to the system without water at 200 ps, this trend inverses at 400 ps and 800 ps as the amount of C, O slows down in the 15% water case compared to 0% case which keeps its past. In the following, we discuss the evolution of the simulation in the 3 frames F1, F2 and F3.

3.1. Time frame 1 (from 0 to 200 ps)

In this time frame the corrosion process starts on a Fe surface without prior oxidation, which mimics the condition of the pipeline upon localized oxide scale removal. In time frame 1 (TF1), a similar carbon diffusion rate is observed for different water concentrations, indicating that, in this time interval, H_2O, OH and atomic O concentrations are low to affect significantly the adsorption, dissociation and diffusion of carbon atoms in the bulk (Fig. 2) at the beginning of simulation. This could be due to the relatively clean iron surface and subsurface, where [23] shows that the high O, OH and H_2O concentration on the surface promote CO dissociation. In this time frame most of the dissociated carbon atoms diffuse to the subsurface (see figure S4). The equations below describe the reaction of CO adsorption (1) and (2) dissociation on the surface.

$$CO + * \rightarrow CO^* \quad (1)$$

$$CO^* \rightarrow C^* + O^* \quad (2)$$

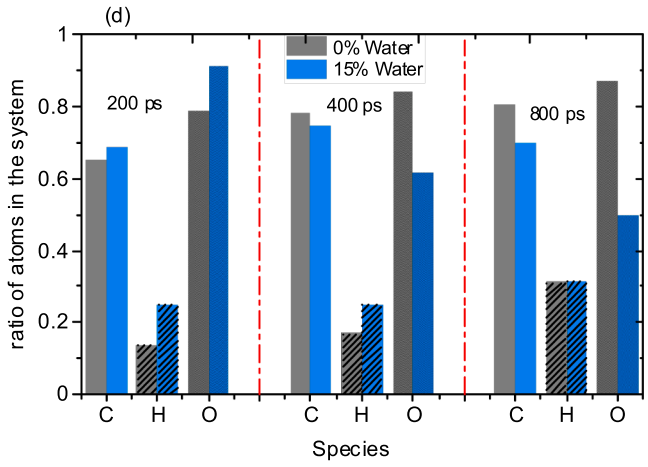

Fig. 4. The fraction of C, H, O atom having diffused from surface to Fe bulk for the system containing15% water (blue) and no water (grey) at 200 ps, 400 ps and 800 ps. By definition, these fractions are undefined at 0 ps.

After adsorption, a part of the water molecules dissociates into H^+ and OH^-. With more OH^- radical on the surface than H_2O (less than 0.20 monolayer ML of water) at 200 ps (Fig. 3-a), we can conclude that the first hydrogen dissociation of water molecule is easier than the second hydrogen dissociation at this stage. Adsorbed and dissociated hydrogen atoms do stay on the surface but diffuse rapidly into the iron bulk (Fig. 4-a). In rare cases, H interact with dissociated C atoms, forming FeCH, thereby stopping free C* atoms from diffusion to the subsurface (Fig. 3-a). Hence, we can summarize remaining reactions in TF1 as:

$$H_2O(g) \rightarrow OH^{-*} + H^{+*} \quad (3)$$

$$H_{2(ad)} \rightarrow H^* + H^* \quad (4)$$

$$H^* + C^* \rightarrow CH^* \quad (5)$$

At the beginning of TF1, we have a Fe surface with CO, H_2O and H_2 molecules adsorbed, consistent with many DFT studies [4,7,23–27]. We can see from Fig. 4 that the amount of H, O and somehow C having diffused is slightly larger in the presence of water at the end of TF1. This can be explained as in [23], where the author compared, using DFT, dissociation of CO, OH, H_2O, CO_2, and H_2 on clean and Fe(1 1 0) surfaces covered with H_2O and OH molecules: the presence of H_2O and OH on a clean Fe surface promotes catalytic reactions by lowering dissociation barriers. The higher OH concentration on Fe surface in TF1 (Fig. 2-a) is likely due to the high barrier required for dissociating the second hydrogen atom of water, a barrier that reaches 0.79 eV at its minimum [26], as compared to 0.35 eV at its minimum when water dissociates on the surface, forming OH* +H* [26].

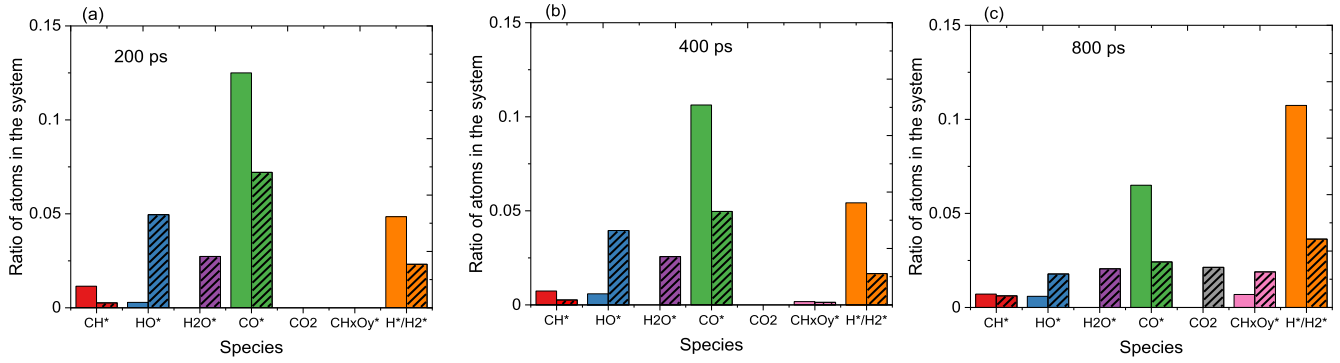

Fig. 3. The fraction of molecules adsorbed/formed on the Fe surface at (a) 200 ps, (b) 400 ps and (c) 800 ps simulation time, the cases with 15% water have sparse pattern, while for 0% water case have no pattern.

3.2. Time frame 2 (200 ps to 400 ps)

In TF2, the amount of diffused C and O without water increases faster than with 15% water (Fig. 4). It shows that while the ratio decreases for the cases with water, the case without water gets an increasing ratio. This change in ratio comparing to TF1 is mainly a result of the blocked CO molecules from adsorbing on the surface due to OH, H_2O molecules. By the end of TF1, the ratio of OH, H_2O molecules at the surface reach 0.02, more than double the fraction of all non-CO molecules in 0% water case. The effect of OH, H_2O on blocking CO molecules from adsorbing on iron surface becomes more noticeable in the TF2 as the trajectories diverge and a decline in C diffusion speed for the systems with the water content is observed (Fig. 2). This is correlated with the increasing content of water on the surface as the difference of OH^- radical in the surface between water/no water cases (Fig. 4-b) at the end of TF1 is important, it starts with 20 OH at 200 ps and reach 35 OH molecule on the surface at 400 ps, compared to the rare OH for the case without water up to 4 OH (see supplementary S4). The effect of OH^- radical in blocking the CO adsorption on the iron surface can be quantified by the enhanced concentration of C, O atomic species contained in the vacuum (See Figure S3). Fig. 3 (a-b) shows the bar chart of molecules at the beginning and end of this frame. The formation of OH molecules on the surface in the absence of water is small (around 0.025). The following reactions start to kick at TF2 associated with the water case as found in Fig. 3 are:

$$H_2O^* \rightarrow OH^* + H^* \quad (7)$$

$$CO^* + H^* \rightarrow CHO \quad (8)$$

$$C^* + H^* \rightarrow CH^* \quad (9)$$

The formation of CHO in reaction (8) can be attributed to a weakening of the C-O bond due to the protonation of C, which makes carbon lose its triple bond with oxygen giving it more ability to capture the H resulting from water dissociation. The presence of water increases hydrogen diffusion. This observation is more evident in figure S4, we can see 40% more H atoms having diffused in the case with water, compared to the case without water despite both being subjected to the same insertion rate/number of H_2 molecules. This trend can also be observed in the normalized results in Fig. 3-b. Stykov el al [28] found that the H_2 dissociation barrier increases from 0.1 eV to 0.6 eV in the presence of pre-adsorbed oxygen atom; they recommended to add pure oxygen to the gas to prevent hydrogen diffusion in iron systems [28]. Another work by S. Liu el al. shows that hydrogen does not adsorb when there is high oxygen concentration on the surface (oxide) [5]. Since we have more oxygen content in the presence of water, hydrogen dissociations could be due to the presence of oxides.

3.3. Frame 3 (400 to 800 ps)

In TF3, the effect of water concentration starts to become more visible, as the effect of different water concentrations on the surface and sub-surface oxidation starts to appear on affecting carbon dissociation and diffusion. The dissociation barrier of water on perfect oxide Fe_3O surface exceeds 1.6 eV as found using DFT calculation [29]. Reaching this level of oxidation will make water prefer to stay on the surface undissociated (as a wetting layer). Even though we don't have a perfect oxide layer. We can see from figure 1 and S5 in the supplementary that the iron surface in TF3 is affected by the oxygen rich layer below the surface, resulting in a higher undissociated water content on the surface (see figure S4-b-c) beside the formation of different hydrocarbon molecules adsorbed at the surface, which tends to deactivate more catalysts sites. Weiss and co-workers [30] showed that oxidized Fe surface act as Lewis acidic surface, by interacting with donor molecules such as H_2O, CO and CO_2 that expose a lone-pair electron through a combination of electrostatics (ion–dipole attraction) and orbital overlap [30]. This condition leads to the formation Carbonic acid (H_2CO_3) that results from the reaction of CO_2 and H_2O on oxidized Fe surface and then can form series corrosive products [31]. Over time, the level of oxidation increases with the water concentration. For example, at 800 ps in the system containing 15% water there are 22.3% O atoms in the bulk, whereas the system containing 3% water contains only 15.5% O atoms (see Figure S3). This oxidation is accompanied by the lower adsorption energy of different gas molecules on the surface as observed by gas reactivity, thus higher dissociation barriers of CO and H_2, as proved by other DFT works [7]. The main reactions are the following:

Without water

$$Fe_xC + CO^* \rightarrow Fe_{x+1}C + O^* \quad (10)$$

$$FeC + C^* \rightarrow FeC_2 \quad (11)$$

$$C^* + O^* + H_2 \rightarrow CH^* + HO^* \quad (12)$$

$$H_2 \rightarrow H^* + H^* \quad (13)$$

With water

$$H_2O + CO \rightarrow CHO + OH \quad (14)$$

$$CHO + C^* + O^* + H^* \rightarrow C_xH_yO_z \quad (15)$$

$$CO^* + O^* \rightarrow CO_2 \quad (16)$$

$$FeC + C^* \rightarrow FeC_2 \quad (17)$$

An opposite trend affects carbon diffusion in the absence of water. That is caused by carbon itself, which forms a thin carbon rich layer near the surface as presented by LDF in figure S4, where we can see a peak of carbon content near the surface. Broos el al [17] have performed a detailed theoretical evaluation of the catalytic nature of low Miller-index surfaces of the Θ-Fe_3C using DFT and conclude that pre-activation of CO is important for lowering of the overall activation barrier. Their work further shows that the high temperature makes Θ-Fe_3C phase highly active towards CO bond dissociation, which is the essential first step in the Fischer–Tropsch reaction. This explains our observation that the speed of CO dissociation reaction increases in the case of 0% TF2 and TF3 to the opposite in the cases with water see Fig. 4. We are not sure if this continues after TP4, as a carbon rich phase starts to form above the surface.

Zou *et al* [13] explored the complex iron surface catalytic chemistry of H_2 and CO using ReaxFF and found that lower barrier essential for methane and simple hydrocarbon (like COOH) formation on Fe (1 0 0) slab [13] using the same reactive force field used here for the surface region. They found that the catalytic surface hydrogenation initiates from the undissociated CO molecules absorbed on the surface of the catalyst as described in the oxygenate mechanism. This process leads to the generation of surface absorbed CHX– groups, which initiates the synthesis of methane and the hydrocarbon chain growth. Zou *et al.* observation is also confirmed here by the different hydrocarbon molecules found, especially in the 15% case (see Fig. 3-c).

3.4. Atom diffusion

We calculated the mean square displacement of C, O and H in pure Fe bulk for a simulation time of 260 ps. Figure S7-b compares carbon diffusion in Fe, Fe_3O_4 and $FeHO_2$ using Extended-ReaxFF for 160 ps. We used the procedure proposed by Guocai et al [32] with a conventional Fe supercell of 12x12x12 and 36 impurity atoms introduced randomly in interstitial sites, leading to an impurity concentration of 1%. Such a large cell and high number of impurities is necessary to get averaged smooth Mean Square Displacement (MSD) curves for reactive MD simulation for simulation time in the range of picoseconds. We calculated the diffusion coefficient for C, H and O in Fe using equation $D = \frac{\langle R^2 \rangle}{6t}$, where $\langle R^2 \rangle$ is the MSD of all atoms, and t is the simulation time.

Figure S7-a shows the fast hydrogen diffusion compared to oxygen

and carbon in pure iron as well known. The diffusion coefficients obtained are $D_0(C) = 5.3 \times 10^{-10}$ cm^2/s, $D_0(O) = 19 \times 10^{-10}$ cm^2/s and $D_0(H) = 63 \times 10^{-10}$ cm^2/s at 773 K. Zhang *et al.* [32] reported that the diffusion coefficient of H atom in pure Fe was $10^{-5} \sim 10^{-8}$ cm^2/s at room temperature measured experimentally [33]. However, the diffusion coefficient of H in theoretical calculation was 10^{-9} 10^{-10} cm^2/s, For carbon, C.S. Becquart *et al.* found $D_0(C) = 1.36 \times 10^{-10}$ cm^2/s using Embedded Atom method [34], while experimental finding varies from 0.39×10^{-11} cm^2/s to 0.16×10^{-11} cm^2/s [35]. It should be noted that, due to a ReaxFF artifact related to the description of a coordinate bond as mentioned by [36], carbon diffusion, in our simulations, is accelerated compared to the real case scenario. For oxygen the experimental results vary largely, from 0.1×10^{-8} cm^2/s to 3.7×10^{-11} cm^2/s [35] depending on the iron sample used. Our results are intended to give a qualitative view only, and they show that these diffusion rates agree with the time formed in our system with faster carbon diffusion that maybe related to the multi grain boundaries system. figure S5 present a linear distribution function of diffused atoms in Fe system, this figure shows a hydride scale from (-10 to −25 Å) oxide scale from (-25 to-35 Å) and a mixed oxide carbide layer (-35 Å to the surface).

Figure S7 shows how the relatively slow C diffusion compared to that of H or O in Fe is fast compared to the diffusion of C in the oxide Fe_3O_4 and the hydroxide $FeHO_2$ materials. The results indicate to what extent pure iron facilitates carbon diffusion compared to when an oxide scale is formed, and how negligible carbon diffusion takes place when reaching the perfect oxide phase as can be seen also in Figure S7-b. It shows also that the presence of hydrogen in the oxide scale helps carbon diffusion compared to the pure oxide scale. DorMohammadi *et al.* noted that iron in neutral (pH = 7) water is not expected to produce a well-structured protective film environment [41]. The oxides that form under these conditions are the result of the active corrosion process; therefore, they are expected to be involved in a mixture of various oxides that are not fully coordinated. The same remark applies to our systems as shown in (Fig. 4-a-b) where we cannot see a well-structured phase.

3.5. Charge map

Fig. 5 shows the relative charge of C, H, O and Fe represented in gray, blue, red and orange respectively, after 800 ps for the two systems with 15% H_2O (a) and without H_2O (b). The increase in the oxide layer density (in red) caused by the presence of water is clearly visible in (Fig. 5b), as well as the high number of hydrocarbon molecules formed above the surface and the molecules formed in the gas phase.

Evaluating the charge along the z-direction underlines how the unreacted hydrogen molecules (which have a relative charge 0) in the gas dissociate and take the charges from the Fe atoms when diffusing to the bulk. They stabilize below 20 Å of the surface forming a hydride layer with a relative charge of 0.18 ± 0.02 eV. Hydrogen atoms cannot get 0.18 eV charge when they are in the iron oxide layer as we see in blue dots in the region −10–0 Å where H change values and could even take positive values in the highly oxide/carbide layer near the surface (Fig. 5). This inability of H to take full charge could explain why hydrogen cannot be stabilized in the Fe-oxide layer and rapidly diffuses into the bulk. Moreover, the increasing presence of oxygen atoms on the surface and in the subsurface layers takes electrons from Fe, thus increasing the Fe surface total positive charge which reaches a relative charge (total charge gained) average of 0.25 eV/0.38 eV for an Fe_S in systems of 0% / 15% water content, respectively at 800 ps (Fig. 4). This Fe positive charge increases the hydrogen gas dissociation barrier and, thus, lowers H diffusion into the bulk. We can distinguish four charge behaviors of C atoms in Fig. 5-b corresponding to the different environments carbon can encounter. The first one is in the bulk region where carbon diffuse into interstitial sites with relative charge of −0.6 ± 0.1 eV, with no C-C or C-O interaction in Fe matrix. The second charge behavior is when C is in interstitial position near oxygen atoms, where it takes a relative charge of −0.45 ± 0.05 eV which is expected as oxygen is more electronegative than carbon. The third charge behavior is near the surface where there is larger C concentration that corresponds to the formation of metallic carbides Fe_xC_y with relative charge of −0.2 ± 0.1 eV. The fourth charge behavior corresponds to carbon taking a positive charge value of + 0.2 ± 0.2 eV as a result of C interaction with surrounding oxygen atoms in Fe poor environment or in vacuum forming CO_2 molecule for example. We can see that Fe atoms always take positive charge due to their metallic bonds with all diffusing atoms, and its relative charge will add up with all diffusing gas atoms leading eventually to zero (unreacted system).

The major difference between the two systems (0% and 15% water concentration at 800 ps) is the considerable hydrogen positive charge of + 0.3 ± 0.05 eV, and oxygen −0.6 ± 0.1 eV in the surface and vacuum regions for the case with water. This charge is an indication of OH, CO_2 and other CH_xO_y formation from the dissociated molecules. The more positive the surface charge, (like in the case of water) the more depleted

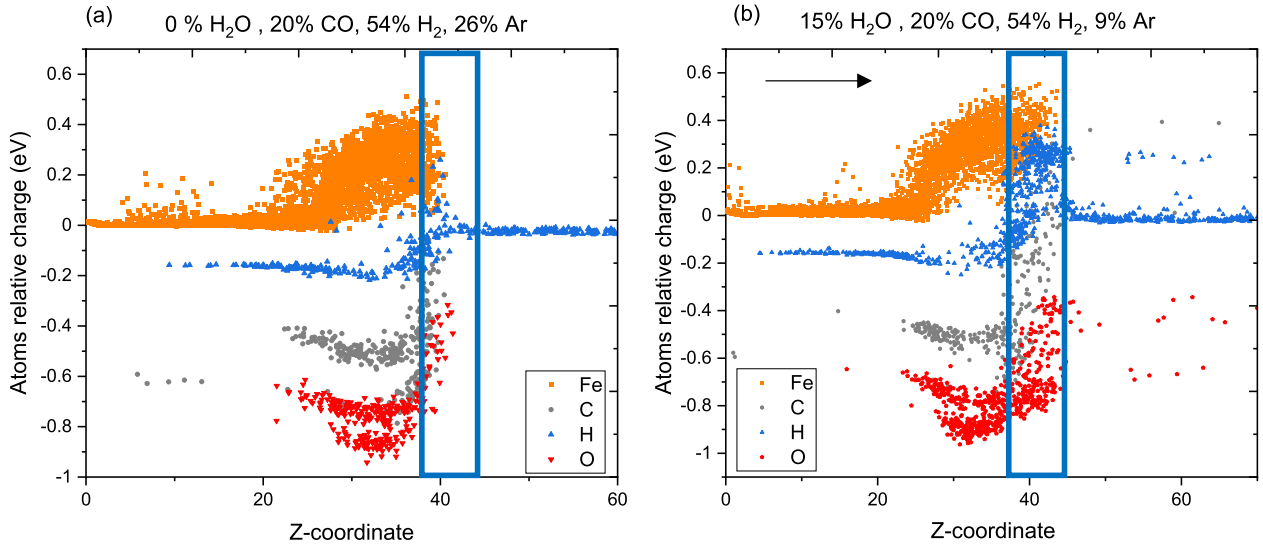

Fig. 5. Charge distributions along the z-direction for C, H,O and Fe at 800 ps and T = 773 K: (a) with no water, (b) 15% water. Gray dots represent charges for the carbon atoms, blue for hydrogen, red oxygen and orange for iron. The blue solid rectangle represents the Fe surface region, the black arrow indicates the direction from bulk to the surface.

the layer catalytic energy thus the lower the absorption energies for new syngas molecules. We can confirm this observation in figure S8 that shows top and side views of the charge density variation map. In the absence of water, the surface remains suitable for carbon dissociation and diffusion as the charges are around zero even at 1200 ps. With water, the surface charge is positive (orange color) leading to very weak CO adsorption and thus higher dissociation barriers as explained by DFT calculations [5,37]. It should be noted that the emerging GBs leads to a much higher CO dissociation rate compared to the perfect surface as discussed in our pervious paper [18]. We did study the carbon diffusion on Fe (1 1 0) surface, we avoided to study this case for the time been because of the inconclusive results due to the small number of carbon atom diffused in this simulation time compared to the 6 grains system. Further studies of the effect of emerging grain boundaries on carbon diffusion from syngas are planned.

This work represents first steps taken towards developing a systematic understanding of atomistic mechanisms governing carburization of steel as a function of gas environment composition. We show that presence of water in the syngas alters the surface state of steels rendering it less susceptible for CO dissociation, and consequently towards carburization. We note that our work most closely mimics the transient processes occurring over relatively fast time-scales of ns for realistic gaseous compositions and conditions of industrial relevance. Potential extension of the accessible time-scale via accelerated multi-scale approaches will be required in describing the transient to steady-state transition of the surface layer.

4. Conclusion

We have used molecular dynamics simulation to study the effect of water concentration on metal dusting corrosion in iron. The Extended-ReaxFF potential used with its enhanced carbon adsorption dissociation and diffusion gave us the possibility to study the effect of water on carbon diffusion for the first time. We used a multi-grain iron system exposed to syngas-like environment at 773 K with a variety of water concentration. Each simulation setup has been run 3 times and the results were averaged in order to verify MD fluctuation associated with each water concentration. We found that water presence reduces carbon diffusion in iron bulk in agreement with experimental observation of Grabke et al. However, the time scale of experiments is several orders of magnitude higher than our simulation making the quantitative comparison unfeasible. During the relatively short simulation time we found that water slows but does not stop carbon diffusion to the bulk. Using a linear distribution function and quantitative study of the diffusion of C/H/O on different mediums, we described the formation of mixed hydride and oxide/carbide layers in iron system. From diffusion analysis, we suggest that hydrogen can have an embrittlement effect on the protective oxide layer as it allows carbon to diffuse faster to the bulk. From the charge maps we found that carbon can take different charge values, an indication of the different bonds type carbon can make from interaction with one oxygen atom in the gas to be in octahedral site in iron matrix. We showed quantitively the evolution of system at distinguishing 3 frames. Using different MD approaches supported by DFT works from literature, we showed how the CO, H2O, H2 adsorption and dissociation barriers change from frame to frame as the iron surface chemistry change with time. We find that after Frame 1, the oxidation in the system without water leads to a thin carbide layer below the surface, leading to an enhancement in a catalytic reaction toward CO molecules. Contrary to the case with water, where the presence of the oxide layer case a high concentration of undissociated OH and H_2O molecules on Fe surface, blocking the Fe catalytic sites thus reducing CO adsorption and dissociation. A future task is to study the diffused rate at longer simulation time P4, where the corrosion product become more prominent.

CRediT authorship contribution statement

El Tayeb Bentria: Investigation, Methodology, Visualization, Data curation, Resources. **Salawu Omotayo Akande:** Resources. **Abitha Ramesh:** Conceptualization, Investigation. **Nicholas Laycock:** Conceptualization, Investigation. **Wouter Hamer:** Investigation, Methodology. **Mousseau Normand:** Methodology, Resources, Supervision. **Becquart Charlotte:** Methodology, Resources, Supervision. **Othmane Bouhali:** Project administration, Conceptualization, Supervision. **Fedwa El-Mellouhi:** Project administration, Resources, Conceptualization, Supervision, Methodology.

Declaration of Competing Interest

The authors declare that they have no known competing financial interests or personal relationships that could have appeared to influence the work reported in this paper.

Acknowledgements

This work is supported by the Qatar National Research Fund (QNRF) through the National Priorities Research Program (NPRP) under project number NPRP10-0105–170118. The advanced computing facility of Texas A & M University at Qatar is used for all calculations. FE and OB are thankful to fruitful discussions with Dr. Prathamesh Shenai, from Shell. Open Access funding is provided by the Qatar National Library

Appendix A. Supplementary material

Supplementary data to this article can be found online at https://doi.org/10.1016/j.apsusc.2021.152138.

References

[1] A.M. El-Sherik, Trends in oil and gas corrosion research and technologies: Production and transmission, Woodhead Publishing, 2017.
[2] H.J. Grabke, C.B. Bracho-Troconis, E.M. Müller-Lorenz, Metal dusting of low alloy steels, Mater. Corros. 45 (4) (1994) 215–221.
[3] K. Natesan, Study of metal dusting phenomenon and development of materials resistant to metal dusting, Argonne National Lab, IL (US), 2002.
[4] R.R.Q. Freitas, R. Rivelino, F. de Brito Mota, C.M.C. de Castilho, Dissociative adsorption and aggregation of water on the Fe (100) surface: a DFT study, J. Phys. Chem. C. 116 (38) (2012) 20306–20314.
[5] S. Liu, Y.-W. Li, J. Wang, H. Jiao, Reactions of CO, H2O, CO2, and H2 on the Clean and Precovered Fe (110) Surfaces–A DFT Investigation, J. Phys. Chem. C. 119 (51) (2015) 28377–28388.
[6] S.O. Akande, E.T. Bentria, O. Bouhali, F. El-Mellouhi, Searching for the rate determining step of the H2S reaction on Fe (110) surface, Appl. Surf. Sci. 532 (2020), 147470.
[7] S. Liu, X. Tian, T. Wang, X. Wen, Y.-W. Li, J. Wang, H. Jiao, Coverage dependent water dissociative adsorption on the clean and O-precovered Fe (111) surfaces, J. Phys. Chem. C. 119 (21) (2015) 11714–11724.
[8] D.J. Dwyer, S.R. Kelemen, A. Kaldor, The water dissociation reaction on clean and oxidized iron (110), J. Chem. Phys. 76 (1982) 1832–1837.
[9] S. Liu, X. Tian, T. Wang, X. Wen, Y.-W. Li, J. Wang, H. Jiao, Coverage dependent water dissociative adsorption on Fe (110) from DFT computation, Phys. Chem. Chem. Phys. 17 (14) (2015) 8811–8821.
[10] T.P. Senftle, S. Hong, M.M. Islam, S.B. Kylasa, Y. Zheng, Y.K. Shin, C. Junkermeier, R. Engel-Herbert, M.J. Janik, H.M. Aktulga, The ReaxFF reactive force-field: development, applications and future directions, Npj Comput. Mater. 2 (2016) 15011.
[11] K. Chenoweth, A.C.T. van Duin, W.A. Goddard, ReaxFF reactive force field for molecular dynamics simulations of hydrocarbon oxidation, J. Phys. Chem. A. 112 (5) (2008) 1040–1053.
[12] J.E. Mueller, A.C.T. van Duin, W.A. Goddard, Development and validation of ReaxFF reactive force field for hydrocarbon chemistry catalyzed by nickel, J. Phys. Chem. C. 114 (11) (2010) 4939–4949.
[13] C. Zou, A.C.T. van Duin, D.C. Sorescu, Theoretical investigation of hydrogen adsorption and dissociation on iron and iron carbide surfaces using the ReaxFF reactive force field method, Top. Catal. 55 (5-6) (2012) 391–401.
[14] E.T. Bentria, S.O. Akande, C.S. Becquart, N. Mousseau, O. Bouhali, F. El-Mellouhi, Capturing the Iron Carburization Mechanisms from the Surface to Bulk, J. Phys. Chem. C. 124 (52) (2020) 28569–28579.
[15] H.M. Aktulga, J.C. Fogarty, S.A. Pandit, A.Y. Grama, Parallel reactive molecular dynamics: Numerical methods and algorithmic techniques, Parallel Comput. 38 (2012) 245–259.

[16] L.R. Williams, L.A. Dykhno, T.J. Hanratty, Droplet flux distributions and entrainment in horizontal gas-liquid flows, Int. J. Multiph. Flow. 22 (1) (1996) 1–18.
[17] R.J.P. Broos, B. Klumpers, B. Zijlstra, I.A.W. Filot, E.J.M. Hensen, A quantum-chemical study of the CO dissociation mechanism on low-index Miller planes of Θ-Fe3C, Catal. Today. 342 (2020) 152–160.
[18] A. Chakrabarty, E.T. Bentria, S.A. Omotayo, O. Bouhali, N. Mousseau, C. S. Becquart, F. El Mellouhi, Elucidating the role of extended surface defects at Fe surfaces on CO adsorption and dissociation, Appl. Surf. Sci. 491 (2019) 792–798.
[19] H.J. Grabke, No Title, Oxid. Met. 39 (1993) 437.
[20] C. Chun, J. Mumford, T. Ramanarayanan, On the mechanism of metal dusting corrosion, in: High Temp. Mater. Proc. a Symp. Honor 65th Birthd. Profr. Wayne L. Worrell, The Electrochemical Society, 2002: p. 247.
[21] A. Stukowski, Visualization and analysis of atomistic simulation data with OVITO–the Open Visualization Tool, Model. Simul. Mater. Sci. Eng. 18 (2009) 15012.
[22] H.J. Grabke, C.B. Bracho-Troconis, E.M. Müller-Lorenz, No Title, Mater. Corros./Werkstoffe Korros. 45 (1994) 215.
[23] S. Liu, Y.-W. Li, J. Wang, H. Jiao, Reactions of CO, H2O, CO2, and H2 on the Clean and Precovered Fe(110) Surfaces - A DFT Investigation, J. Phys. Chem. C. 119 (51) (2015) 28377–28388, https://doi.org/10.1021/acs.jpcc.5b0749710.1021/acs.jpcc.5b07497.s001.
[24] C.-H. Zhang, B. Chen, D.-B. Sun, A DFT study of H2O dissociation on metal-precovered Fe (100) surface, Surf. Interface Anal. 50 (4) (2018) 420–429.
[25] F. Mirabella, E. Zaki, F. Ivars-Barceló, X. Li, J. Paier, J. Sauer, S. Shaikhutdinov, H.-J. Freund, Cooperative Formation of Long-Range Ordering in Water Ad-layers on Fe3O4 (111) Surfaces, Angew. Chemie Int. Ed. 57 (5) (2018) 1409–1413.
[26] S.C. Jung, M.H. Kang, Adsorption of a water molecule on Fe (100): Density-functional calculations, Phys. Rev. B. 81 (2010), 115460.
[27] D.E. Jiang, E.A. Carter, Adsorption, diffusion, and dissociation of H2S on Fe (100) from first principles, J. Phys. Chem. B. 108 (50) (2004) 19140–19145.
[28] A. Staykov, J. Yamabe, B.P. Somerday, Effect of hydrogen gas impurities on the hydrogen dissociation on iron surface, Int. J. Quantum Chem. 114 (10) (2014) 626–635.
[29] S. Yin, X. Ma, D.E. Ellis, Initial stages of H2O adsorption and hydroxylation of Fe-terminated α-Fe2O3 (0 0 0 1) surface, Surf. Sci. 601 (12) (2007) 2426–2437.
[30] W. Weiss, W. Ranke, Surface chemistry and catalysis on well-defined epitaxial iron-oxide layers, Prog. Surf. Sci. 70 (1-3) (2002) 1–151.
[31] V.-A. Glezakou, L.X. Dang, B.P. McGrail, Spontaneous activation of CO2 and possible corrosion pathways on the low-index iron surface Fe (100), J. Phys. Chem. C. 113 (9) (2009) 3691–3696.
[32] G. Lv, M. Zhang, H. Zhang, Y. Su, Hydrogen diffusion and vacancy clusterization in iron, Int. J. Hydrogen Energy. 43 (32) (2018) 15378–15385.
[33] K. Kiuchi, R.B. McLellan, The solubility and diffusivity of hydrogen in well-annealed and deformed iron, Perspect. Hydrog. Met. (1986) 29–52.
[34] C.S. Becquart, J.M. Raulot, G. Bencteux, C. Domain, M. Perez, S. Garruchet, H. Nguyen, Atomistic modeling of an Fe system with a small concentration of C, Comput. Mater. Sci. 40 (1) (2007) 119–129, https://doi.org/10.1016/j.commatsci.2006.11.005.
[35] L. Claire, Numerical Data and Functional relationship is science and technology, Landolt-Bo¨rnstein, New Ser. III (26) (1990) 480–481.
[36] S.J. Pai, H.W. Lee, S.S. Han, Improved Description of a Coordinate Bond in the ReaxFF Reactive Force Field, J. Phys. Chem. Lett. 10 (22) (2019) 7293–7299.
[37] C. Huo, J. Ren, Y. Li, J. Wang, H. Jiao, CO dissociation on clean and hydrogen precovered Fe (111) surfaces, J. Catal. 249 (2) (2007) 174–184.